New Journal of Physics
The open–access journal for physics

Coupling biochemistry and mechanics in cell adhesion: a model for inhomogeneous stress fiber contraction

Achim Besser and Ulrich S Schwarz[1]
University of Heidelberg, Bioquant, BQ 0013 BIOMS Schwarz,
Im Neuenheimer Feld 267, D-69120, Heidelberg, Germany
E-mail: Ulrich.Schwarz@bioquant.uni-heidelberg.de

New Journal of Physics **9** (2007) 425
Received 3 July 2007
Published 30 November 2007
Online at http://www.njp.org/
doi:10.1088/1367-2630/9/11/425

Abstract. Biochemistry and mechanics are closely coupled in cell adhesion. At sites of cell-matrix adhesion, mechanical force triggers signaling through the Rho-pathway, which leads to structural reinforcement and increased contractility in the actin cytoskeleton. The resulting force acts back to the sites of adhesion, resulting in a positive feedback loop for mature adhesion. Here, we model this biochemical–mechanical feedback loop for the special case when the actin cytoskeleton is organized in stress fibers, which are contractile bundles of actin filaments. Activation of myosin II molecular motors through the Rho-pathway is described by a system of reaction–diffusion equations, which are coupled into a viscoelastic model for a contractile actin bundle. We find strong spatial gradients in the activation of contractility and in the corresponding deformation pattern of the stress fiber, in good agreement with experimental findings.

[1] Author to whom any correspondence should be addressed.

PII: S1367-2630(07)54065-6

Contents

1. Introduction 2
2. Biochemical model for the Rho-pathway 6
3. Sarcomeric unit of stress fiber model 13
4. Continuum version of stress fiber model 15
5. Role of feedback 18
6. Conclusion 24
Acknowledgments 24
References 24

1. Introduction

Adhesion of biological cells to each other and the extracellular matrix is one of the hallmarks of multicellular organisms and a very active area of research in cell biology. Investigating cell adhesion is crucial to understand physiological processes like tissue development and maintenance, but also disease-related processes like growth and migration of cancer cells [1, 2]. In general, biological cells have a limited repertoire of possible behaviors, including spreading, adhesion, migration, division or death, but very sophisticated ways of controlling the switching between these different processes. Traditionally, investigation of this cellular decision making has focused strongly on the biochemical aspects, including detailed models for signal transduction [3, 4]. During recent years, it has become increasingly clear that in adhesion-related processes, cellular behavior is not only controlled by biochemical cues, but also involves many physical determinants like the structural organization of the extracellular matrix and the cytoskeleton or force generation through molecular motors [5]–[8]. For example, it has been shown that the stiffness of the extracellular environment determines migration of tissue cells [9] and differentiation of stem cells [10]. In particular, these cellular responses have been found to depend on the ability of the cells to contract their environment with actomyosin contractility and to convert this mechanical process into a biochemical signal. Although these processes are essential for such important situations like tissue functioning or cancer cell migration, theoretical models describing the coupling between biochemistry and mechanics in cell adhesion are still rare, albeit essential for a future systematic understanding of how multicellular organisms organize themselves.

Cell adhesion is closely related to the actin cytoskeleton, whose organization is central in determining the structural properties of cells. In cell culture with stiff substrates, the actin cytoskeleton tends to organize in *stress fibers*, which are bundles of actin filaments tensed by myosin II molecular motors [11]. Stress fibers usually end in *focal adhesions*, which are integrin-based adhesion contacts which can grow to a lateral size of several microns [12, 13]. On their cytoplasmic side, focal adhesions recruit more than 90 components (mostly proteins) which physically reside in the adhesion structure [14]. In 1992, Ridley and Hall published a landmark paper demonstrating that the assembly of stress fibers and focal adhesions is regulated by a small GTPase called Rho [15]. Rho has many isoforms, but the one mainly associated with focal adhesions is RhoA, which for simplicity in the following we referred to as Rho. In a companion paper of the same year, Ridley *et al* [16] showed that another small GTPase called Rac stimulates the formation of lamellipodia as they appear in cell migration. The main

isoform associated with focal adhesions is Rac1 which for simplicity in the following we will refer to as Rac. While Rho mainly acts through activation of actomyosin contractility, the main effect of Rac is activation of actin polymerization, in particular activation of the actin nucleation factor Arp2/3. It has been reported later that activation of Rac downregulates Rho, leading to disassembly of stress fibers and focal adhesions [17]. In many situations, Rho and Rac can be regarded as antagonists, switching the cytoskeleton between different structural states [18]. They are part of a larger family of small GTPases, called the Rho-family, which for example also includes Cdc42, which stimulates the formation of filopodia and maintains cell polarity [19]. Apart from regulation of the actin cytoskeleton, the small GTPases from the Rho-family have many other functions in the cell, for example in cell cycle control and differentiation.

Although the small GTPases from the Rho-family are simple molecular switches, they are regulated by many different factors. In general, GTPases are upregulated by guanine nucleotide exchange factors (GEFs), which convert the inactive Rho-GDP form to the active Rho-GTP form by exchanging GDP for GTP. They are downregulated by GTPase-activating proteins (GAPs), which stimulate Rho-GTPase activity, thus leading to GTP-hydrolysis and transforming the active Rho-GTP to the inactive Rho-GDP. For the 20 members of the Rho-family, 60 different GEFs and 70 different GAPs as well as more than 60 different downstream targets have been identified [20]. At the current stage of affairs, there is no way how this complex network can be modeled in full detail. However, certain parts of this network have been well characterized by biochemical assays, in particular different parts of the Rho-mediated signal transduction pathway leading from focal adhesions to actomyosin contractility.

Here, we focus on the role of Rho as a stabilizing factor for mature adhesion. During recent years, it has been shown that Rho is the central component of a biochemical–mechanical feedback loop which regulates mature adhesion. In detail, it has been shown that application of force on focal adhesions triggers their growth in a Rho-dependent manner [21] (reviewed in [13, 18]). Two main downstream targets of Rho leading to stress fiber formation have been identified. The formin mDia leads to actin polymerization, while the Rho-associated kinase (ROCK) leads to phosphorylation of myosin light chain (MLC) and thus to increased motor activity. Together these effects lead to the formation of and contractility in stress fibers and therefore to increased force levels at focal adhesions. In this way, a positive feedback loop is closed for upregulation of mature adhesion characterized by focal adhesions and stress fibers. This biochemical–mechanical feedback loop is schematically depicted in figure 1. An essential part of this feedback loop is the growth of focal adhesion under force, which recently has been the subject of different modeling approaches [22]–[27] (reviewed in [28]). However, these models have focused mainly on the mechanical and thermodynamic aspects of the growth process, neglecting the interaction of mechanics and biochemical signaling. The positive feedback loop between contractility and growth of adhesions has been modeled before in the framework of kinetic equations, but without addressing the details of force generation and its regulation by signaling pathways [29]. Similar kinetic equations have been used to model the antagonistic roles of Rho and Rac in cell adhesion, but again without addressing the details of force generation and regulation [30]. Recently force generation has been addressed in more detail in a model for whole cell contractility and stress fiber formation [31, 32]. However, no details of the signaling pathway have been modeled except for an unspecified activation signal.

Because the actin cytoskeleton is very dynamic and interacts with many different molecular factors, including actin-associated proteins and molecular motors, it is very difficult to model its

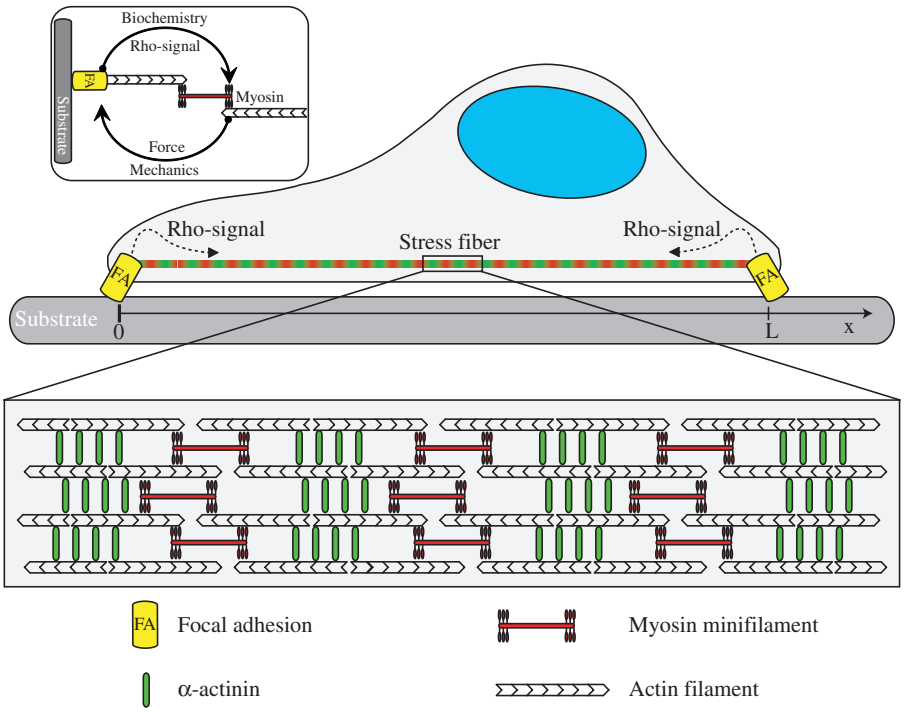

Figure 1. Cells adhere to the extracellular matrix by integrin-mediated contacts called focal adhesions. These contacts are the anchor points of stress fibers, which are actin filament bundles held together by the crosslinker molecule α-actinin and myosin II molecular motors. The myosins are assembled in myosin mini-filaments. Due to myosin motor activity stress fibers are under tension and exert forces to focal adhesions. This mechanical stimulus initiates biochemical signals (Rho-signal) that originate from focal adhesions and propagate into the cytoplasm, altering in turn myosin activity. Therefore the system of focal adhesions and stress fibers are connected by a biochemical and mechanical positive feedback loop (inset). The spatial part of our model is 1D with one stress fiber extending between the two focal adhesions at $x = 0$ and $x = L$.

mechanical properties in a general way. However, modeling becomes feasible if one focuses on one of the well-characterized states of the actin cytoskeleton, for example the lamellipodium or stress fibers. Because here we are mostly interested in mature cell adhesion in culture, we will focus on the latter case. Modeling stress fibers can be approached from different perspectives. An obvious starting point are their common characteristics with muscle fibers, which is a linear sequence of sarcomeres, each containing around 300 myosin II molecular motors working collectively together as they slide the actin filaments relatively to each other. This field has been pioneered by the Huxley model [33], which later has been modified in many regards, e.g. in regard to filament extensibility [34] or by a detailed modeling of the myosin II hydrolysis cycle [35]. In contrast to muscle fibers, stress fibers are more disordered and a complete description therefore requires a model for their assembly process from polar filaments interacting through molecular motors. Such a description has been achieved in the framework of a phenomenological theory which however does not model the details of the underlying motor

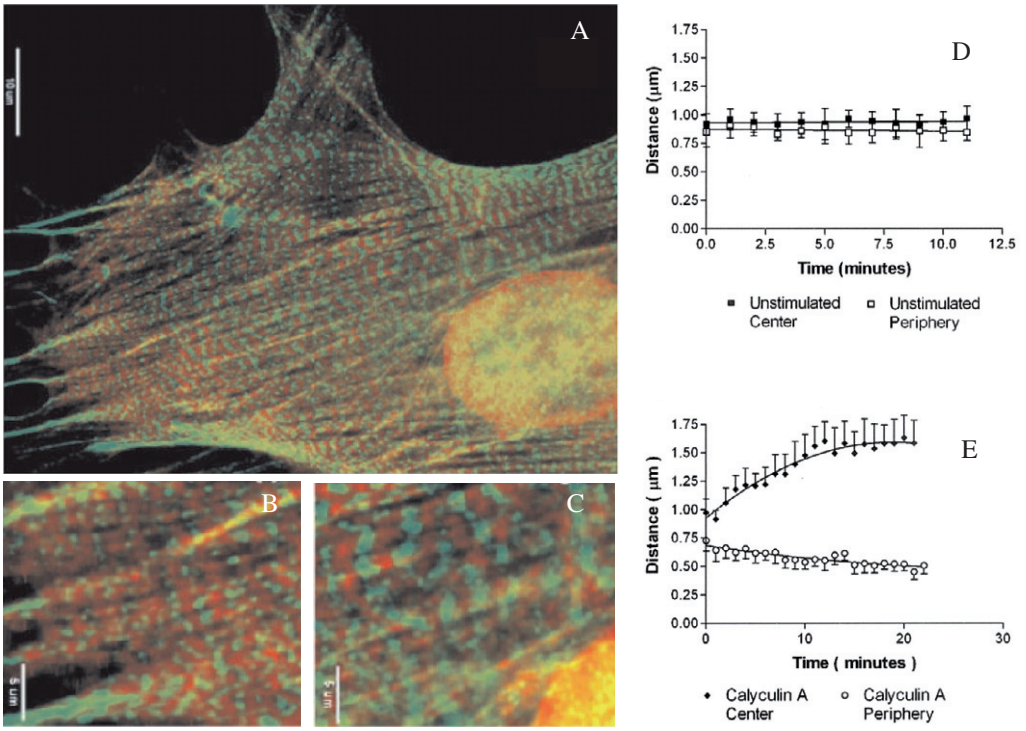

Figure 2. (A) Peterson *et al* [38] studied the deformation of stress fibers in fibroblasts by using fluorescently labeled α-actinin (in green) and MLC (in red). These two components arrange sequentially along the stress fibers and thereby form regular striation patterns. Myosin contractility was stimulated with the drug calyculin A. Then an inhomogeneous striation pattern results: stress fibers contract at the cell periphery (B) but expand at the cell center (C). These results were quantified by time course measurements of the mean pattern bandwidths in the respective regions. Compared with the control (D), stimulation of contractility leads to very strong spatial gradients (E) on the timescale of tens of minutes.

activity [36, 37]. This theory does predict different dynamical states of the system, including a stationary state of isometric contraction as observed in stress fibers.

Although less ordered than muscle on the level of electron microscopy, stress fibers do exhibit a periodic organization. Figure 2 shows experimental data for fibroblast adhesion to a stiff substrate [38]. The image of a whole cell shown in figure 2(A) reveals a banding pattern in the stress fibers. The green regions correspond to the actin crosslinker α-actinin while the red regions correspond to myosin II molecular motors. Non-muscle myosin II is known to assemble into bipolar minifilaments consisting of 10–30 myosins, as depicted in the cartoon of a stress fiber in figure 1. In contrast to muscle, the striation pattern of stress fibers shows considerable variability along the length of a stress fiber. In particular, it has been observed that upon stimulation of contraction with the drug calyculin A, only the sarcomeres in the periphery (close to the focal adhesions, figure 2(B)) shorten, while those in the center (close to the cell body, figure 2(C)) elongate. The exact time course of the striation width is shown in figures 2(D) and (E) for control and stimulation experiments, respectively. This demonstrates that activation

of contractility leads to strong spatial gradients in the striation pattern. Thus, it is not sufficient to model only one sarcomeric unit as it is typically done for muscle [33]–[35]. Rather at least a one-dimensional (1D) chain of such sarcomeres has to be considered.

Here, we introduce a new 1D model for stress fibers which essentially models them as linear sequence of viscoelastic Kelvin–Voigt bodies, whose stationary state is determined by the elastic part. The action of the molecular motors inside each sarcomeric unit are included on the level of a linearized force–velocity relationship. The signaling pathway is modeled as a system of reaction–diffusion equations. For this study, we have conducted an extensive survey of the relevant literature and have collected the measured rate and diffusion constants in such a way that they now can be used for mathematical modeling. The coupling between the biochemical signaling pathway and the mechanical stress fiber model proceeds by introducing a spatially varying fraction of active molecular motors. The local activation level is thereby determined by the outcome of the signaling pathway. A continuum limit of the mechanical model for many sarcomeric units in series results in a partial differential equation with mixed derivatives. The whole system of reaction–diffusion equations for the signal transduction and the partial differential equation for the mechanical part can be solved simultaneously. By feeding the force resulting from the mechanical model back into the activation of the signaling pathway, we obtain for the first time a model for the closed biochemical–mechanical feedback cycle described above. As a first application of our model, here, we show that it predicts heterogeneous contraction of stress fibers, in good agreement with experiments. In general, our work shows how models for the coupling of biochemistry and mechanics can be devised in a meaningful way.

The paper is organized as follows. In section 2, we start with our model for the part of the Rho-pathway which is relevant for our purposes. We then introduce our mechanical model for one sarcomeric unit of the stress fibers in section 3 and its continuum limit for a whole stress fiber in section 4. In section 5, our model predictions for inhomogeneous contraction upon activation of contractility by calyculin are compared to the experimental results. Finally, we conclude in section 6.

2. Biochemical model for the Rho-pathway

In this study, we concentrate on stress fibers and their regulation by the Rho-pathway. In figure 1, we introduce a coordinate system for our 1D model: the stress fiber extends along the positive x-direction and the endpoints at $x = 0$ and $x = L$ correspond to two focal adhesions. Because the two focal adhesions are treated as equivalent, our model has inflection symmetry around $x = L/2$. In figure 3, we schematically depict the biochemical part of our model in the spatial context of the focal adhesion at $x = 0$ (by symmetry, the same description applies to the one at $x = L$). Three compartments have to be considered: the focal adhesion, the cytoplasm and the stress fiber. In our model, each of these compartments corresponds to one or two important biochemical components. The reaction pathway is a linear sequence of activating or inhibitory enzyme reactions initiated at focal adhesion, transmitted through the cytoplasm by diffusion and resulting in spatially dependent myosin activation in the stress fiber. In the following we discuss each reaction step in detail and show how these processes are translated into reaction–diffusion equations. The abbreviations used for the biochemical components are compiled in table 1, together with a short description of their functions. The model equations are summarized in table 2.

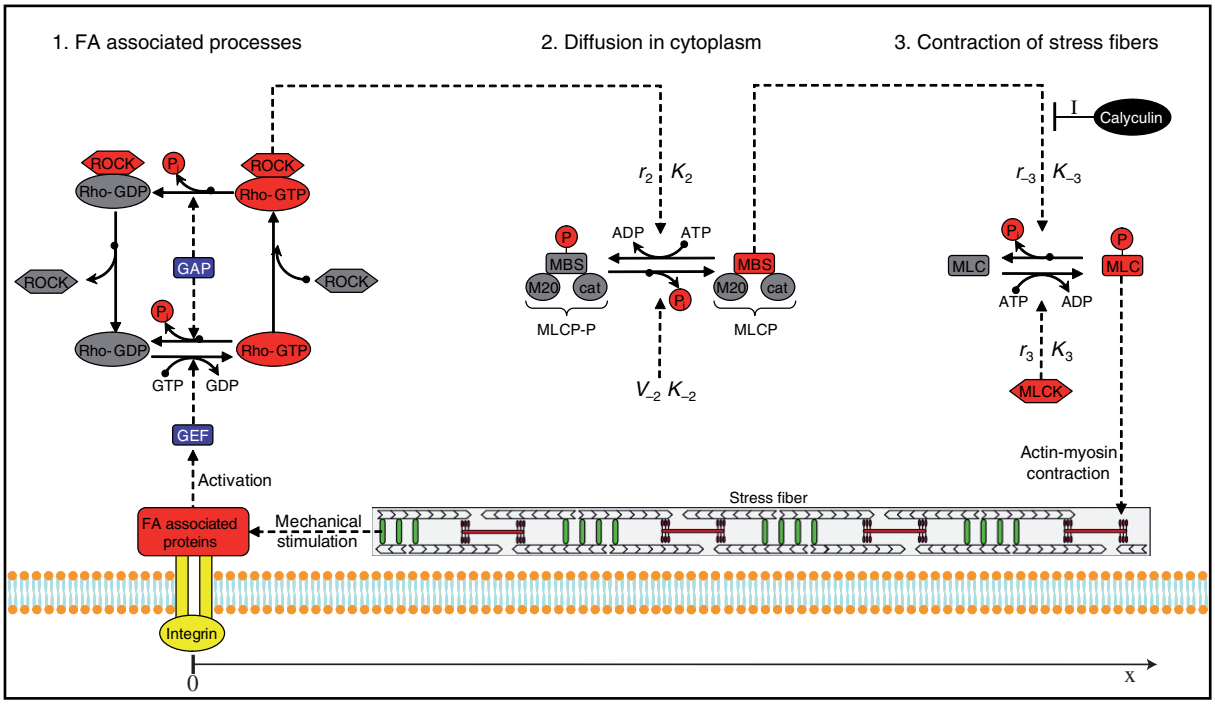

Figure 3. Signaling pathway that controls myosin contractility depicted in its appropriate spatial context: mechanical cues are transduced to various biochemical signals at focal adhesions, however the precise mechanisms have not been resolved yet. One possible mechanism is that a Rho-GEF is activated by a mechanosensitive process at focal adhesions. Rho-GEF then promotes Rho-GTP loading and subsequent complexation with ROCK which gets activated. Active ROCK is able to phosphorylate MLCP at its MBS. MLCP and MLCP-P are freely diffusible in the cytoplasm and thus can reach the myosins in the stress fibers. Increased phosphorylation of MLCP to MLCP-P by ROCK effectively leads to increased phosphorylation of MLC, thus increasing myosin contractility.

Our modeling of the biochemical signaling pathway starts with the activation of Rho at focal adhesions. The Rho-protein has a lipophilic end that serves to anchor it to lipid membranes [39]. Complexation with guanine nucleotide dissociation inhibitors (GDIs) shields the hydrophobic parts of the Rho-protein and make it inactive as well as soluble in the cytoplasm [40]. It is expected that Rho is released from these complexes at focal adhesions. More importantly, focal adhesions are known to recruit different Rho-GEFs, thus activating Rho at the focal adhesions. The active Rho is then able to bind ROCK and thereby activate its kinase activity [41]. Since the active ROCK is bound to Rho-GTP, we assume in our model that these components are not diffusible but are localized to the focal adhesions. For the same reason, we neglect the direct interaction of ROCK and myosin which has been reported to occur *in vitro*. Active ROCK phosphorylates the diffusible myosin light chain phosphatase (MLCP) at its myosin-binding subunit (MBS). MLCP and its antagonistic partner myosin light chain kinase (MLCK) are the main regulators of myosin contractility in the context we are interested in. Both enzymes interact with the regulatory MLC subunit of the myosins. Depending on the respective activities, MLC gets either phosphorylated or dephosphorylated. MLC, in turn, controls the

Table 1. Abbreviations and full names of the biochemical components. For each component, a short description of its function is given.

Abbreviation	Full name	Function
GDP/GTP	Guanosine diphosphate/guanosine triphosphate	Small molecule without and with a third phosphate group, energy source of conformational changes
GEF	Guanine nucleotide exchange factor	Activates GTPases by exchanging GDP for GTP
GAP	GTPase-activating protein	Stimulates GTP-hydrolysis, converting active GTPases (GTP-bound) to their inactive (GDP-bound) form
GDI	Guanine nucleotide dissociation inhibitor	Binds to inactive form of GTPases, the complex is soluble in the cytoplasm
MLC	Myosin light chain	Subunit of myosin II molecular motors, regulates myosin binding to actin filaments
MLCK	Myosin light chain kinase	Phosphorylates MLC
MLCP	Myosin light chain phosphatase	Dephosphorylates MLC
MLCP-P	Phosphorylated MLCP	Inactive form of MLCP
MBS	Myosin-binding subunit	Subunit of MLCP whose phosphorylation makes MLCP inactive
ROCK	Rho-associated kinase	ROCK phosphorylates MLCP at its MBS
I	Effect of calyculin	Inhibits MLCP from dephosphorylating myosin, thus enhancing contractility

myosin binding to actin filaments. Only if MLC is phosphorylated is myosin able to bind actin filaments and perform its ATPase cycle that converts chemical energy into mechanical work, e.g. contraction of stress fibers [42]. By phosphorylating MLCP, ROCK effectively enhances the phosphorylation level of MLC. In this way, Rho-activation can lead to an increase in myosin contractility in the stress fiber.

Our model for the biochemical reaction–diffusion system assumes that each enzyme stimulation follows Michaelis–Menten kinetics [43]. In Michaelis–Menten kinetics, production first increases linearly with educt concentration and then saturates at a maximal production velocity if educt concentration exceeds the value set by the Michaelis–Menten constant. The precise molecular process corresponding to the conversion of force into a biochemical signal at focal adhesions has not been identified yet. However, it is expected that mechanical forces exerted on to focal adhesions eventually initiate the loading of Rho-GTP leading to ROCK activation. For lack of information we therefore lump the focal adhesion associated processes into one equation that effectively describes the conversion of ROCK into its activated form (presumably complexed with Rho-GTP). The mechanical force F_b that stimulates the activation is treated as enzyme in the framework of Michaelis–Menten kinetics:

$$\frac{\partial \mathrm{ROCK}(t)}{\partial t} = \frac{r_1 F_b(t)(\mathrm{ROCK}_{tot} - \mathrm{ROCK}(t))}{K_1 + (\mathrm{ROCK}_{tot} - \mathrm{ROCK}(t))} - \frac{V_{-1}\mathrm{ROCK}(t)}{K_{-1} + \mathrm{ROCK}(t)}. \quad (1)$$

The variable ROCK denotes the activated form of ROCK and we assume that the overall concentration of ROCK is constant at ROCK_{tot}. The force exerted by the stress fiber on to the focal adhesion, $F_b(t)$, stimulates the conversion of ROCK into its activated form with maximum velocity $r_1 F_b(t)$ and Michaelis–Menten constant K_1. The parameter r_1 is equivalent to a

Table 2. Summary of model equations. Equations (m1)–(m4) describe successive biochemical signaling events: (m1) focal adhesion associated activation of ROCK; (m2) and (m3) phosphorylation and diffusion of MLCP and dephosphorylation and diffusion of MLCP-P; (m4) regulation of the active fraction of the myosins, which is identified with the phosphorylated fraction of MLC. Equation (m5) is the mechanical model equation for stress fibers, where $u(x,t)$ is the displacement along the fiber. The boundary conditions for the partial differential equations (m2), (m3) and (m5) are given by (bc2), (bc3) and (bc5), respectively. In equation (bc2) and (bc3), the upper (lower) sign is valid for the left $x = 0$ (right $x = L$) boundary. For the sake of clarity, we have introduced the listed abbreviations for the stall force F_{stall}, the effective viscosity η_{e} and the force exerted on to the boundary F_{b}. The presented results have been derived with the assumptions that: (I) the diffusion properties of the phosphorylated and unphosphorylated form of the phosphatase are the same, hence $D = D_{\text{p}}$. (II) The viscoelastic properties of the stress fiber do not vary in space, therefore $k(x) \to k$ and $\eta_{\text{e}}(x,t) \to \eta + F_{\max}\, n(x,t)/v_0$.

Model equations

$$\frac{\partial \text{ROCK}(t)}{\partial t} = \frac{r_1 F_{\text{b}}(t)(\text{ROCK}_{\text{tot}} - \text{ROCK}(t))}{K_1 + (\text{ROCK}_{\text{tot}} - \text{ROCK}(t))} - \frac{V_{-1}\text{ROCK}(t)}{K_{-1} + \text{ROCK}(t)} \tag{m1}$$

$$\frac{\partial \text{MLCP}(x,t)}{\partial t} = \frac{V_{-2}\text{MLCP-P}(x,t)}{K_{-2} + \text{MLCP-P}(x,t)} + D\frac{\partial^2 \text{MLCP}(x,t)}{\partial x^2} \tag{m2}$$

$$\frac{\partial \text{MLCP-P}(x,t)}{\partial t} = -\frac{V_{-2}\text{MLCP-P}(x,t)}{K_{-2} + \text{MLCP-P}(x,t)} + D_p\frac{\partial^2 \text{MLCP-P}(x,t)}{\partial x^2} \tag{m3}$$

$$\frac{\partial n(x,t)}{\partial t} = \frac{V_3\,(1 - n(x,t))}{K_3 + (1 - n(x,t))} - \frac{r_{-3}\text{MLCP}(x,t)n(x,t)}{K_{-3}I + n(x,t)} \tag{m4}$$

$$\left(\frac{\partial}{\partial x}\eta_{\text{e}}(x,t)\frac{\partial}{\partial x}\frac{\partial}{\partial t} + \frac{\partial}{\partial x}k(x)\frac{\partial}{\partial x}\right)u(x,t) = -\frac{1}{a}\frac{\partial}{\partial x}F_{\text{stall}}(x,t) \tag{m5}$$

Boundary conditions at $x = 0, L$

$$\frac{\partial \text{MLCP}(x,t)}{\partial x} = \pm\frac{V_2}{D}\frac{\text{ROCK}(t)\text{MLCP}(x,t)}{K_2 + \text{MLCP}(x,t)} \tag{bc2}$$

$$\frac{\partial \text{MLCP-P}(x,t)}{\partial x} = \mp\frac{V_2}{D_p}\frac{\text{ROCK}(t)\text{MLCP}(x,t)}{K_2 + \text{MLCP}(x,t)} \tag{bc3}$$

$$u(x,t) = 0 \quad \text{Stiff boundaries} \tag{bc5}$$

Abbreviations

$$F_{\text{stall}}(x,t) = F_{\max}\, n(x,t)$$

$$\eta_{\text{e}}(x,t) = \eta(x) + F_{\text{stall}}(x,t)/v_0$$

$$F_{\text{b}}(t) = a\eta_{\text{e}}(0,t)\partial_x\partial_t u(0,t) + ak(0)\partial_x u(0,t) + F_{\text{stall}}(0,t)$$

rate constant but relates mechanical force to a chemical reaction. For this reason the units of r_1 are given as [nM/s nN]. The force $F_b(t)$ will depend on the stress fiber deformation. The second term accounts for the degradation of activated ROCK to its inactive form, with maximum velocity V_{-1} and Michaelis–Menten constant K_{-1}. Since we expect ROCK in its active form to be associated with focal adhesions, we omit diffusive contributions to this equation.

One main effector of ROCK is MLCP which we regard as a diffusible compound leading to a reaction–diffusion equation:

$$\frac{\partial \mathrm{MLCP}(x,t)}{\partial t} = \frac{V_{-2}\mathrm{MLCP\text{-}P}(x,t)}{K_{-2}+\mathrm{MLCP\text{-}P}(x,t)} + D\frac{\partial^2 \mathrm{MLCP}(x,t)}{\partial x^2}. \tag{2}$$

Here, the variables MLCP-P and MLCP denote the phosphorylated and unphosphorylated form of MLCP, respectively. The first term accounts for the dephosphorylation of MLCP-P with maximum velocity V_{-2} and Michaelis–Menten constant K_{-2}. The second term allows for the diffusion of the phosphatase with diffusion constant D. The phosphorylation level of MLCP is also regulated by the active form of ROCK which catalyzes the reverse reaction, i.e. the conversion of the phosphatase into its phosphorylated form. However, ROCK is active only in the vicinity of focal adhesions located at each end of the stress fiber. Therefore, this source term can be incorporated into the boundary conditions for equation (2), in the sense that the diffusive flux into the boundary has to balance the conversion into its inactive form:

$$D\frac{\partial \mathrm{MLCP}(x=0,t)}{\partial x} = \frac{R_2\mathrm{ROCK}(t)\mathrm{MLCP}(x=0,t)}{K_2+\mathrm{MLCP}(x=0,t)}. \tag{3}$$

The same relation, but with inverted sign is valid at the other end at $x = L$, compare the overview in table 2. The reaction is again modeled with Michaelis–Menten kinetics, where $R_2 = r_2 v_b$ is the product of a rate constant r_2 with an effective volume v_b of the focal adhesion in which the reaction takes place. K_2 is the usual Michaelis–Menten constant. For the phosphorylated form of the phosphatase (MLCP-P) equations similar to equations (2) and (3) are valid, but with inverted signs of the source terms and a diffusion constant which in principle can be different, see table 2.

MLCP together with MLCK regulates the phosphorylation level of MLC. Since myosins in stress fibers form mini-filaments which are bound to actin filaments, we neglect diffusion of this compound, leading to the rate equation for the phosphorylated fraction n of MLC:

$$\frac{\partial n(x,t)}{\partial t} = \frac{V_3\,(1-n(x,t))}{K_3+(1-n(x,t))} - \frac{r_{-3}\mathrm{MLCP}(x,t)n(x,t)}{K_{-3}\;I+n(x,t)}. \tag{4}$$

By allowing only the ratio of the phosphorylated fraction to vary, we assume that the overall amount of myosin in the stress fibers is fixed. MLC is phosphorylated by MLCK with a maximum velocity $V_3 = r_3\mathrm{MLCK}$ and respective Michaelis–Menten constant K_3. Here, we assume that the concentration of MLCK is constant within the cell. The kinase is antagonized by MLCP that dephosphorylates MLC with a rate constant r_{-3} and Michaelis–Menten constant K_{-3}. The factor I is an inhibition parameter defined below. Since MLCP has spatial-dependent source terms and is diffusible, the inhibition of MLC by the phosphatase will vary in space.

To complete the biochemical modeling, we have to specify how the induction of calyculin is treated in our model. Calyculin is an inhibitor of MLCP and thereby enhances the phosphorylation level of MLC. We model the interaction of calyculin with its target MLCP as a competitive inhibition leading to the additional factor I in the last term of equation (4) [44].

Table 3. Model parameters based on literature search. We have set the model parameters such that they fit into the reported range. The equation for the phosphorylated fraction of MLC is normalized to the total myosin concentration denoted by M. In order to make the involved reaction constant comparable to the literature values we give K_3, K_{-3}, r_3 and r_{-3} scaled with M. Equation (1) translates mechanical forces into biochemical activation. For this reason the units of the rate constant r_1 are given as [nM s^{-1} nN^{-1}]. The typical relaxation time, τ, of stress fibers is of the order of a few seconds [45] therewith we roughly estimate the viscosity value as $\eta \approx \tau k$ where we use $\tau = 1$ s. Myosin activation by calyculin is modelled as competitive inhibition of the phosphatase. The inhibition parameter I is switched instantaneously from $I = 1$ to $I = 3$. Some of the reported values have been measured for the interactions of protein fractions and not for the native proteins. Furthermore, the experiments have been done on proteins extracted from different species.

Abbreviation	Meaning	Used value	Reference values	References
Time dependent reaction variables				
ROCK	Activated form of ROCK	$0 \ldots 5$ nM	$\gtrsim 1$ nM	[41]
MLCP	Unphosphorylated form of MLCP	$0 \ldots 1.2\,\mu$M	$1.2 \pm 0.3\,\mu$M	[46]
MLCP-P	Phosphorylated form of MLCP	$0 \ldots 1.2\,\mu$M	$1.2 \pm 0.3\,\mu$M	[46]
n	Fraction of active myosin	$0 \ldots 1$	[MLC-phos]/[myosin]	
Reaction constants				
MLCK	Myosin light chain kinase	$0.1\,\mu$M	$\gtrsim 100$ nM	[47]
M	Myosin concentration	$30\,\mu$M	$25 \ldots 30\,\mu$M	[48]
K_1	Michaelis constant	5 nM	**(No value)**	
K_{-1}	Michaelis constant	4.7 nM	**(No value)**	
K_2	Michaelis constant	$0.1\,\mu$M	$0.10 \pm 0.01\,\mu$M	[41]
K_{-2}	Michaelis constant	$15\,\mu$M	**(No value)**	
$K_3 * \mathrm{M}$	Michaelis constant	$20\,\mu$M	$52.1 \pm 7.1\,\mu$M	[49]
			$34.5 \pm 2.8\,\mu$M	[41]
			$18\,\mu$M	[50]
			$7.7 \ldots 96.0\,\mu$M	[51]
			$19 \ldots 53\,\mu$M	[47]
			$20\,\mu$M	[52]
$K_{-3} * \mathrm{M}$	Michaelis constant	$10\,\mu$M	$10\,\mu$M	[53]
r_1	Rate constant	0.3 nM s^{-1} nN^{-1}	**(No value)**	
V_{-1}	Maximum velocity	1.8 nM s^{-1}	**(No value)**	
r_2	Rate constant	2.4 s^{-1}	2.36 ± 0.10 s^{-1}	[41]
R_2	Maximum velocity	$4.8\,\mu$m s^{-1}	$r_2 * v_b$	
V_{-2}	Maximum velocity	$0.1\,\mu$M s^{-1}	**(No value)**	
$r_3 * \mathrm{M}$	Rate constant	10 s^{-1}	2.00 ± 0.36 s^{-1}	[49]
			3.85 ± 0.095 s^{-1}	[41]
			5.17 s^{-1}	[50]
			$7.37 \ldots 171.3$ s^{-1}	[51]
			$70 \ldots 100$ s^{-1}	[47]
			4.64 s^{-1}	[52]

Table 3. (Continued.)

Abbreviation	Meaning	Used value	Reference values	References
V_3	Maximum velocity	$1.0\,\mu\mathrm{M\,s^{-1}}$	r_3 * MLCK	
r_{-3} * M	Rate constant	$21\,\mathrm{s^{-1}}$	$21\,\mathrm{s^{-1}}$	[53]
D	Diffusion constant of MLCP and MLCP-P	$14\,\mu\mathrm{m^2\,s^{-1}}$	$10 \ldots 100\,\mu\mathrm{m^2\,s^{-1}}$	[54]
v_b	Effect. react. vol. of FAs	$2.0\,\mu\mathrm{m}$	**(No value)**	
I	Inhibition parameter	$1 \rightarrow 3$	**(No value)**	
Parameters of mechanical model				
F_max	Stall force	50 nN	**(No value)**	
v_0	Maximum motor velocity	$1.0\,\mu\mathrm{m\,s^{-1}}$	$\approx 0.1 \ldots 1\,\mu\mathrm{m\,s^{-1}}$	[55]
a	Vec-element spacing	$1.0\,\mu\mathrm{m}$	$1.0\,\mu\mathrm{m}$	[38]
k	Spring stiffness	$45\,\mathrm{nN}\,\mu\mathrm{m^{-1}}$	$45.7\,\mathrm{nN\,a^{-1}}$	[56]
η	Viscosity	$45\,\mathrm{nN\,s}\,\mu\mathrm{m^{-1}}$	$\approx \tau k = 45.7\,\mathrm{nN\,s\,a^{-1}}$	[45, 56]
L	Fiber length	$50\,\mu\mathrm{m}$	$\approx 20 \ldots 80\,\mu\mathrm{m}$	

In the presence of calyculin $I > 1$ (in absence of the drug: $I = 1$) which effectively increases the Michaelis–Menten constant K_{-3} and thus decreases the rate of MLC dephosphorylation. Hence, more myosin motors will be activated and cell contractility is stimulated. The induction of the drug is then modeled by switching instantaneously the inhibition parameter from $I = 1$ to $I = 3$. Thereby, we omit the time delay caused by the internalization of the drug.

The used parameter values for the reaction–diffusion system are based on an extensive survey of the literature and are summarized in table 3. If a range of values is reported in the literature, we chose an intermediate value for this parameter. If no value could be found in the literature, we made reasonable assumptions based on similar parameters in other systems. No attempt was made to fit the parameters to some target function. We first analyze the properties of this reaction–diffusion system assuming that the boundary force exerted on to the focal adhesions is held at a constant level. This would be the case if the myosin forces were in a stationary state and not regulated by the biochemical signals emerging from focal adhesions. We impose artificial initial conditions that all components (ROCK, MLCP-P and n) are at zero activation level but set the boundary force to 5 nN, a typical force observed for fibroblast [57]. This mechanical stimulation triggers the accumulation of active ROCK at focal adhesions, see equation (1), creating a sink for the active form of MLCP. Thus in those boundary regions MLCK dominates and increases MLC phosphorylation. Closer to the center of the cell MLC rather remains in its unphosphorylated form. The width of the interfacial region of intermediate MLC-phosphorylation level is mainly determined by the diffusiveness of the phosphatase. The faster the diffusion, the wider the intermediate region. On a typical timescale of a few minutes all components equilibrate to their steady state concentration profile, where MLC is highly phosphorylated at the boundaries, but is poorly activated at the center of the stress fiber. In figure 4, we show the typical equilibration of the phosphorylated fraction of MLC, $n(x, t)$, as obtained from a solution of the full system of biochemical reaction–diffusion equations. Below, we will argue that this phosphorylation profile of MLC implies a spatially varying myosin motor activation leading to an inhomogeneous stress fiber contraction.

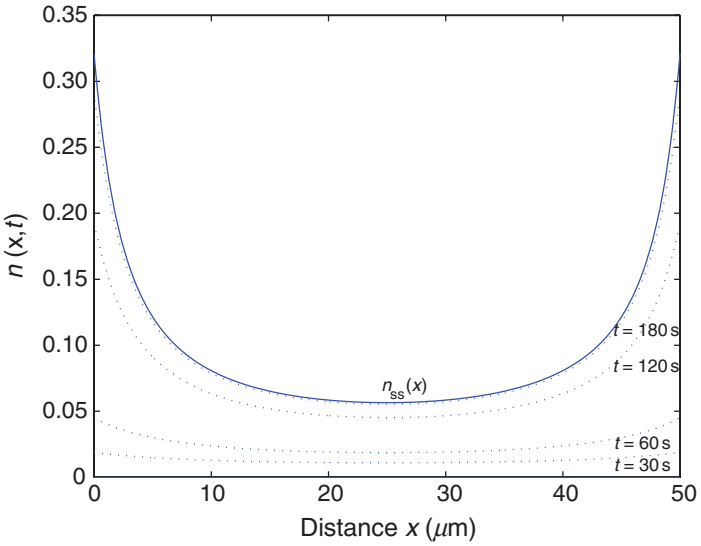

Figure 4. Spatial dependence of the active myosin fraction $n(x,t)$ at four different time points $t \in \{30\,\text{s}, 60\,\text{s}, 120\,\text{s} \text{ and } 180\,\text{s}\}$ as well as for the steady state, $n_{\text{ss}}(x)$: we solve the biochemical model implying the artificial initial conditions that all components are at zero activation level, but set the boundary force to 5 nN. Because of this mechanical trigger at focal adhesions, MLC gets preferentially activated at the boundaries via the Rho-pathway which leads to a steady increase of the myosin activation level. Due to diffusible compounds in the Rho-pathway, the increased activation level is smoothed out towards the center of the cell.

3. Sarcomeric unit of stress fiber model

A minimal model for stress fibers has to take into account not only the viscoelastic but also the contractile properties of the fiber due to myosin motor activity. For the mechanical response of a sarcomeric unit, we take the usual Kelvin–Voigt model for viscoelastic material [58]. It consists of a dashpot with viscosity η and a spring of stiffness k connected in parallel. These two modules represent viscous and elastic properties of the material, respectively. The Kelvin–Voigt model is the simplest viscoelastic model which in the stationary state is determined by elasticity, in contrast to the Maxwell model, which flows in the stationary limit. Thus the Kelvin–Voigt model is the appropriate choice for stress fibers, which can carry load at constant deformation over a long time. In order to cope with the contractile behavior of stress fibers, we introduce an additional contractile element that represents the activity of motor proteins. For illustrative reasons, we first derive the governing differential equation for such a viscoelastic and contractile element (*vec-element*) before we proceed to the stress fiber model. This ansatz is similar to the two-spring model which we have introduced before to explain the physical aspects of rigidity sensing on soft elastic substrates [59].

The considered vec-element is depicted in figure 5. The properties of the additional contractile element is given by the specific force–velocity relation of the molecular motor. For

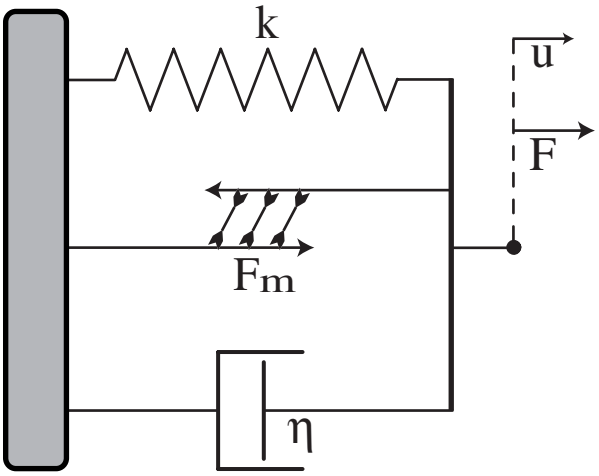

Figure 5. The viscoelastic and contractile element (vec-element) consists of a spring of stiffness k, a contractile module of contraction force F_{m} and a dashpot of viscosity η that are all connected in parallel. Spring and dashpot taken alone are the usual Kelvin–Voigt model of viscoelastic material. The properties of the contractile module are characterized to first-order by the linearized force–velocity relation.

simplicity, we use the linearized relationship:

$$F_{\mathrm{m}}(v) = F_{\mathrm{stall}}\left(1 - \frac{v}{v_0}\right), \tag{5}$$

where F_{m} is the actual force exerted by a motor moving with velocity v. v_0 is the zero-load velocity and F_{stall} is the stall force of the motor, that is the maximal force allowing motor movement. In the following description for the stress fiber, the stall force will depend on the active fraction of the myosin, compare equation (13), such that myosin contractility may vary spatially. The sum of all internal forces, F, exerted by the vec-element reads

$$F = -\eta\frac{\mathrm{d}u}{\mathrm{d}t} - ku - F_{\mathrm{m}}. \tag{6}$$

The crucial point is that the motor force $F_{\mathrm{m}}(v)$ is related to the contraction velocity v which relates to the displacement $u(t)$ simply by

$$v = -\frac{\mathrm{d}u}{\mathrm{d}t}. \tag{7}$$

The minus sign comes from the fact that the directed motor movement causes a relative sliding of the anti-parallel orientated actin filaments leading to contraction of the element with velocity v. Thus the displacement $u(t)$ becomes negative upon motor activity. If there are no external forces, all internal forces have to balance, $F = 0$, and we arrive at the following differential equation for the displacement $u(t)$:

$$\left(\eta + \frac{F_{\mathrm{stall}}}{v_0}\right)\frac{\mathrm{d}u}{\mathrm{d}t} + ku = -F_{\mathrm{stall}}. \tag{8}$$

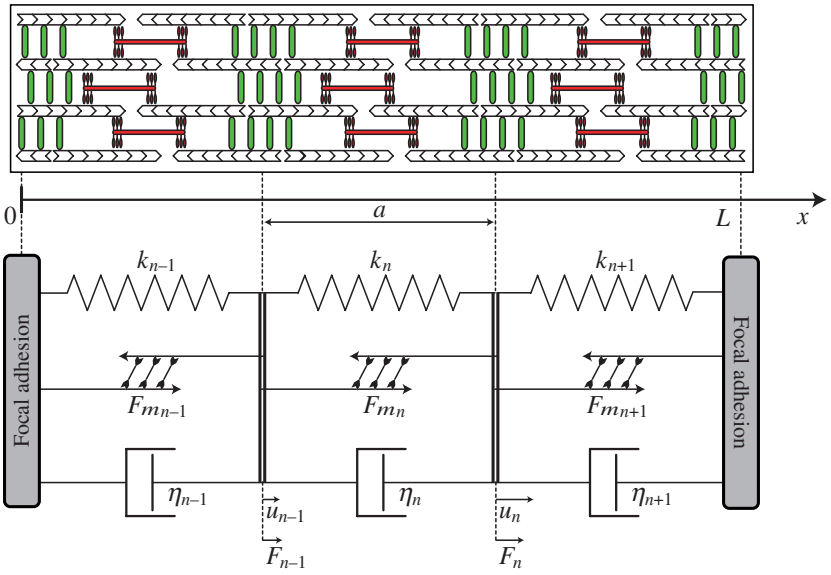

Figure 6. We model a stress fiber as a string of vec-elements such that the spring stiffness k_n, the viscosity η_n and the motor force F_{m_n} can vary spatially, e.g. the latter will vary spatially due to different myosin activity at the periphery compared to the center. The displacement of a certain site n is denoted by u_n. The force F_n on to this site n consists of elastic, viscous and motor contributions, compare equation (10). In the following, we assume fixed boundary conditions, namely $u(0,t) \equiv 0$ and $u(L,t) \equiv 0$ where L is the total length of the fiber.

The term originating from the motor activity decomposes into two contributions. Firstly it increases the viscosity of the damping term (dissipative signature of the motor) and secondly it contributes a constant force to the inhomogeneous part of the equation (contractility of the motor). Assuming vanishing initial displacement $u(t=0)=0$, the solution to equation (8) is given by:

$$u(t) = -\frac{F_{\mathrm{stall}}}{k}\left(1 - \mathrm{e}^{-t/\tau}\right). \tag{9}$$

Here $\tau = \eta_{\mathrm{e}}/k$ corresponds to the relaxation time of the Kelvin–Voigt model with an effective viscosity $\eta_{\mathrm{e}} = \eta + F_{\mathrm{stall}}/v_0$. Thus, the system appears to be more viscous for stronger and slower motors and subsequently the motor activity slows down any relaxation due to perturbations of the system. The steady state deformation $u(t \to \infty) = -F_{\mathrm{stall}}/k$ is determined by the ratio of stall force and spring stiffness.

4. Continuum version of stress fiber model

We model a stress fiber as a string of vec-elements whose viscoelastic and contractile properties may vary spatially. For example the contractile strength of the vec-elements will vary spatially because the biochemical signal will cause different myosin activation levels along the fiber. Starting from a discrete description depicted in figure 6, we derive the governing continuum equation. Similar to the preceding discussion, the force F_n on the site n is the sum of spring

forces, viscous drag and the forces built up by the motor proteins:

$$F_n = \eta_{n+1}\frac{\partial}{\partial t}(u_{n+1}-u_n) - \eta_n\frac{\partial}{\partial t}(u_n-u_{n-1}) + k_{n+1}(u_{n+1}-u_n) - k_n(u_n-u_{n-1}) + F_{\mathrm{m}_{n+1}} - F_{\mathrm{m}_n}. \tag{10}$$

Here, we allow that the stiffness of the spring, the viscosity as well as the motor force vary spatially. In order to deduce a continuum description, we expand the functions η, k, u and F_m at $x = na$ assuming that these functions are smooth within the small distance a. Keeping only leading order terms yields:

$$F(x,t) = a^2\left(\frac{\partial}{\partial x}\eta(x)\frac{\partial}{\partial x}\frac{\partial}{\partial t} + \frac{\partial}{\partial x}k(x)\frac{\partial}{\partial x}\right)u(x,t) + a\frac{\partial F_{\mathrm{m}}(x,t)}{\partial x}. \tag{11}$$

Note that the leading differential operator ∂_x acts on η and u. The same holds for the second term. If k does not vary spatially, it simplifies to $k\partial_x^2$. Like for a single vec-element, we argue that the motor force F_{m} depends on the displacement $u(x,t)$. The contraction Δ_n within the nth element generated by the respective motor is given by $\Delta_n = -(u_n - u_{n-1})$. The contraction velocity is therefore $v(x,t) = \dot{\Delta}(x,t) \approx -a\partial_t\partial_x u(x,t)$. The found expression for the velocity is inserted into the force velocity relation equation (5) leading to:

$$F_{\mathrm{m}}(x,t) = F_{\mathrm{stall}}(x,t)\left(1 + \frac{a}{v_0}\frac{\partial}{\partial t}\frac{\partial}{\partial x}u(x,t)\right). \tag{12}$$

In contrast to equation (5), here the stall force is not constant but depends on the phosphorylated fraction $n(x,t)$ of MLC along the stress fiber. This comes from the fact that along a myosin minifilament and depending on MLC phosphorylation, a larger or smaller fraction of myosin heads is able to bind to actin and perform ATP-cycles. The more myosin heads are active the larger the maximum force that the bundle can exert to the actin filaments. In our model we regard the ensemble of myosins within a cross-section of a stress fiber as one large contractile unit with an effective stall force that depends linearly on the active fraction n of myosin heads:

$$F_{\mathrm{stall}}(x,t) = F_{\max}\, n(x,t). \tag{13}$$

The effective stall force, $F_{\mathrm{stall}}(x,t)$, would reach the maximum force $F_{\max}$ if all myosins within this cross-section would be working ($n = 1$). In the following, we set $F_{\max} = 50\,\mathrm{nN}$ which will result in boundary forces exerted by the fiber of about 5 nN which corresponds to typical values observed in experiments [58]. Equation (11) together with equation (12) and (13) lead to the final model equation for the stress fiber:

$$\left(\frac{\partial}{\partial x}\eta_{\mathrm{e}}(x,t)\frac{\partial}{\partial x}\frac{\partial}{\partial t} + \frac{\partial}{\partial x}k(x)\frac{\partial}{\partial x}\right)u(x,t) = -\frac{1}{a}\frac{\partial}{\partial x}F_{\mathrm{stall}}(x,t), \tag{14}$$

where the effective viscosity $\eta_{\mathrm{e}}(x,t) = \eta(x) + F_{\mathrm{stall}}(x,t)/v_0$ is similar to the findings in equation (8), although here the viscosity varies spatially. Interestingly, only the variation of the motor force appears on the right-hand side of the equation. As a consequence, a homogeneous motor activity will not contribute to the displacements within the string.

To obtain some intuition for this equation, assume that the spatially varying stall force is given, e.g. by the steady state solution n_{ss} of the reaction–diffusion system, depicted in figure 4,

such that $F_{\mathrm{stall}}(x) = F_{\max} n_{\mathrm{ss}}(x)$. For this simplifying case where the stall force does not vary in time, equation (14) can be integrated and the time-dependent solution for $u(x,t)$ is given by:

$$u(x,t) = u(x_0,t) + \int_{x_0}^{x} \mathrm{d}x' \left(\partial_{x'} u(x',t_0) \mathrm{e}^{-(t-t_0)/\tau(x')} - \frac{F_{\mathrm{stall}}(x')}{ak(x')} \left[1 - \mathrm{e}^{-(t-t_0)/\tau(x')} \right] + \frac{1}{a\eta_{\mathrm{e}}(x')} \mathrm{e}^{-(t-t_0)/\tau(x')} \int_{t_0}^{t} F_{\mathrm{b}}(t') \mathrm{e}^{(t'-t_0)/\tau(x')} \, \mathrm{d}t' \right). \tag{15}$$

Here, we have set $\tau(x) = \eta_{\mathrm{e}}(x)/k(x)$, the typical relaxation time with which perturbations decay at a certain position. For example the initial conditions $\partial_x u(x,t_0)$ can be regarded as perturbations to the steady state and they decay with $\exp(-t/\tau(x))$. The three integration constants can be identified as the displacement at the left boundary, $u(x_0,t)$, the force exerted to the left boundary, $F_{\mathrm{b}}(t)$, and the initial strain along the fiber, $\partial_x u(x,t_0)$. They are determined by the boundary and initial conditions. Experiments by Peterson *et al* [38] are arranged with cells on stiff substrates to which the ends of the stress fiber are connected by focal adhesions. Therefore, the appropriate boundary conditions are fixed ends for the fiber, namely $u(x_0,t) \equiv 0$ and $u(x_{\mathrm{e}},t) \equiv 0$. From the second condition, one is able to calculate the missing integration constant $F_{\mathrm{b}}(t)$ for any initial condition $\partial_x u(x,t_0)$. The force on the left boundary $F_{\mathrm{b}}(t)$ is given as solution to an inhomogeneous Volterra equation of the first kind:

$$\int_{t_0}^{t} K(t-t') F_{\mathrm{b}}(t') \mathrm{d}t' = g(t), \tag{16}$$

with the kernel

$$K(t-t') = \int_{x_0}^{x_{\mathrm{e}}} \mathrm{d}x' \frac{1}{a\eta_{\mathrm{e}}(x')} \mathrm{e}^{-(t-t')/\tau(x')} \tag{17}$$

and an inhomogeneous part $g(t)$ dependent on the initial condition $\partial_x u(x,t_0)$:

$$g(t) = \int_{x_0}^{x_{\mathrm{e}}} \mathrm{d}x' \left(\frac{F_{\mathrm{stall}}(x')}{ak(x')} \left[1 - \mathrm{e}^{-(t-t_0)/\tau(x')} \right] - \partial_{x'} u(x',t_0) \mathrm{e}^{-(t-t_0)/\tau(x')} \right). \tag{18}$$

In order to solve the integral equation (16) for $F_{\mathrm{b}}(t)$, we calculate its time derivative, leading to:

$$F_{\mathrm{b}}(t) = \frac{\dot{g}(t)}{K(0)} - \frac{1}{K(0)} \int_{t_0}^{t} \dot{K}(t-t') F_{\mathrm{b}}(t') \, \mathrm{d}t'. \tag{19}$$

This equation yields an explicit expression for the initial force F_{b} at $t = 0$:

$$F_{\mathrm{b}}(t_0) = \frac{\dot{g}(t_0)}{K(0)} \neq 0. \tag{20}$$

By inspection of the kernel in equation (17) and the inhomogeneous part in equation (18), one finds that the initial force on to the boundary has a finite value, even for the initial condition $\partial_x u(x,t_0) = 0$. Equation (19) also yields an iteration rule for the time course of $F_{\mathrm{b}}(t)$, by applying a quadrature, where $F_{\mathrm{b}}(t_0)$ from equation (20) is used as a starting value. The solution for $F_{\mathrm{b}}(t)$ is shown in figure 7. The boundary force is rising from its initial value and then quickly saturates at about 4.8 nN. The result for $F_{\mathrm{b}}(t)$ can then be set into the general solution (equation (15)) for the displacement $u(x,t)$ along the fiber. Figure 8 shows this solution, by using the steady state activation level for the myosins ($F_{\mathrm{stall}}(x) = F_{\max} n_{\mathrm{ss}}(x)$) shown in figure 4 and assuming the initial condition $\partial_x u(x,t_0) = 0$ as well as the boundary conditions $u(0,t) \equiv 0$

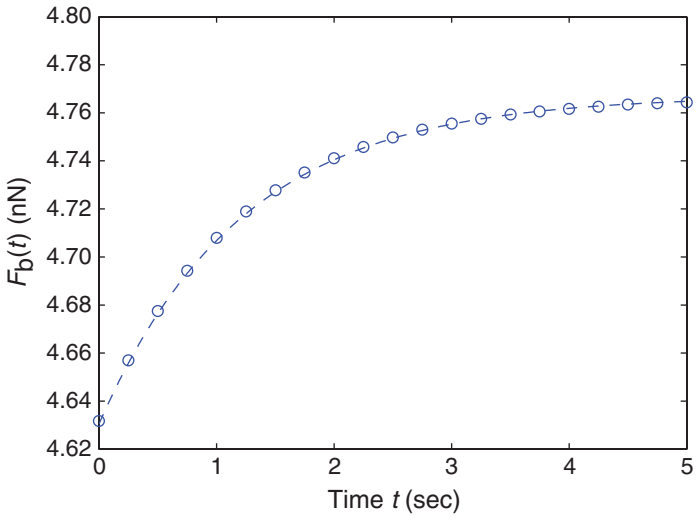

Figure 7. Time course of boundary force $F_b(t)$. The solution of the Volterra equation, equation (16), indicated by circles, was calculated by applying an iteration rule further explained in the main text. The dashed line is the boundary force deduced from direct numerical solution of equation (14) which we include for comparison. For the assumed initial condition, $\partial_x u(x, 0) = 0$, the boundary force increases from its non-zero value at $t = 0$, given by equation (20) and quickly saturates at somehow larger values.

and $u(L, t) \equiv 0$. Beside the analytical solution, indicated by circles, we also included the direct numerical solution of equation (14) for comparison. The numerical solution was derived by using the MATLAB algorithm 'pdepe'. The sinusoidal shape of the function u results from stronger contractile motors close to the boundaries causing the fiber elements to displace into the direction of the boundaries. Hence the displacement u is positive (negative) along the right (left) half of the fiber. It is worth noting that the mechanical equilibration of the stress fiber occurs within seconds in contrast to the biochemical system which equilibrates over minutes.

5. Role of feedback

We already argued that the system of focal adhesions and stress fibers exhibits a closed biochemical and mechanical positive feedback loop. Despite this fact, the previous results were derived under the assumption that the mechanically triggered biochemical signals at FAs originate from a constant force. In order to model the full biological system, the varying boundary forces have to be fed back into the equation describing the mechanotransduction equation (1). Since the stress fiber model does not include any cross-links (e.g. intermediate contacts to the substrate) the tension γ within the fiber has to be constant and therefore equals the boundary forces:

$$F_b(t) = \gamma(x = 0) = a\eta_e(0, t)\partial_x\partial_t u(0, t) + ak(0)\partial_x u(0, t) + F_{stall}(0, t). \qquad (21)$$

This relation now connects the biochemical signaling to the mechanical deformation of the stress fiber. Thus, the coupled system of reaction equations (1)–(4), and the mechanical equation (14) have to be solved simultaneously. This can be done numerically by using the

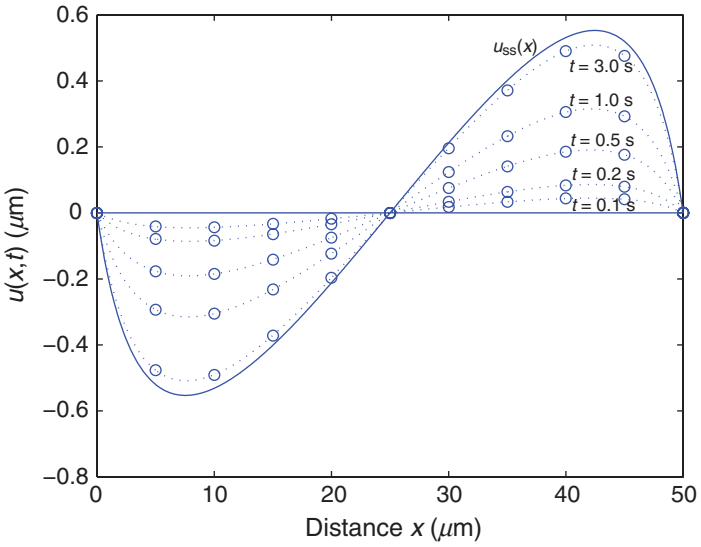

Figure 8. We first analyze the solution of the mechanical equation (14) by assuming a steady state myosin activation level, $n_{ss}(x)$, shown in figure 4. For this simplifying case where the myosin activation level is not time dependent, equation (14) can be solved both numerically and analytically. It shows the analytical solution, equation (15), indicated by circles whereas the direct numerical solution of equation (14) is indicated by dotted lines. The solution is given at time points $t \in \{0.1\,\mathrm{s}, 0.2\,\mathrm{s}, 0.5\,\mathrm{s}, 1.0\,\mathrm{s}$ and $3.0\,\mathrm{s}\}$ as well as for the steady state $u_{ss}(x)$, assuming the initial condition: $\partial_x u(x, 0) \equiv 0$ and the boundary conditions: $u(0, t) \equiv 0$ and $u(L, t) \equiv 0$.

MATLAB algorithm 'pdepe'. The whole system of equations and the used parameter values are summarized in tables 2 and 3, respectively.

By doing a steady state analysis we find that this system of equations exhibits two stable steady states for the used parameter values: the first state is characterized by a generally low activation level $n_{ss}(x)$ of the myosin motors resulting in marginal boundary forces whereas in the second state myosin motors are non-uniformly activated and the exerted forces reach a few nN. This bistability is characteristic for a positive feedback system [3]. The first 'non-active' state would correspond to cells that failed to establish mechanical stress whereas the second 'active' state correspond to cells that are well adhered to the substrate. In order to simulate the drug experiments by Peterson *et al* [38], we start with the system residing in this 'active' state and then, at $t = 0$, we perturb the system by turning on the stimulation with calyculin. This is modeled by switching instantaneously the inhibition parameter from $I = 1$ to $I = 3$, thereby omitting the time delay caused by the internalization of the drug. The stimulation with calyculin reduces the phosphatase activity and elevates the myosin activation level everywhere leading to a quick increase in the boundary forces exerted by the stress fiber. The time course of the force exerted on to the focal adhesions is shown in figure 9. Subsequently, the positive mechanical feedback triggers additional signaling at focal adhesions activating myosin motors preferentially at the cell periphery. This results in strong spatial gradients in myosin motor activity, see figure 11. The strong peripheral motors then contract the fiber to the cost of the central regions where the fiber has to elongate. This can be further analyzed by using the

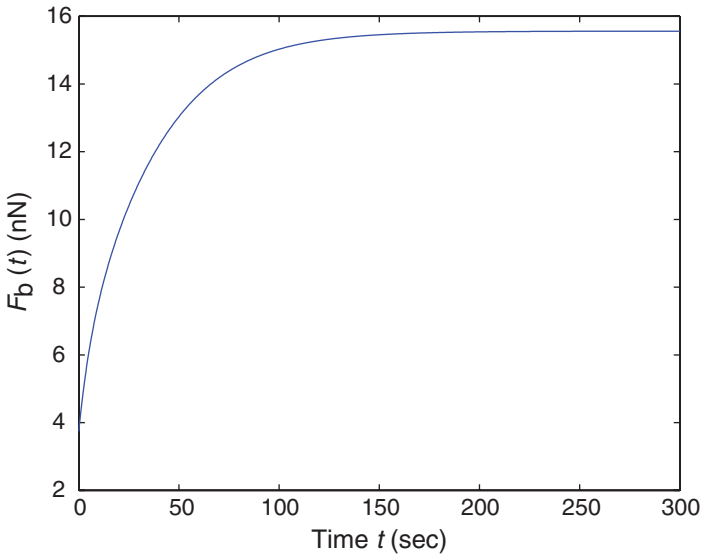

Figure 9. At $t = 0$ calyculin is added to the system. Then myosin motors along the filament get activated and further increase the tension within the fiber. The time course of the force $F_b(t)$ transduced to the boundaries is shown.

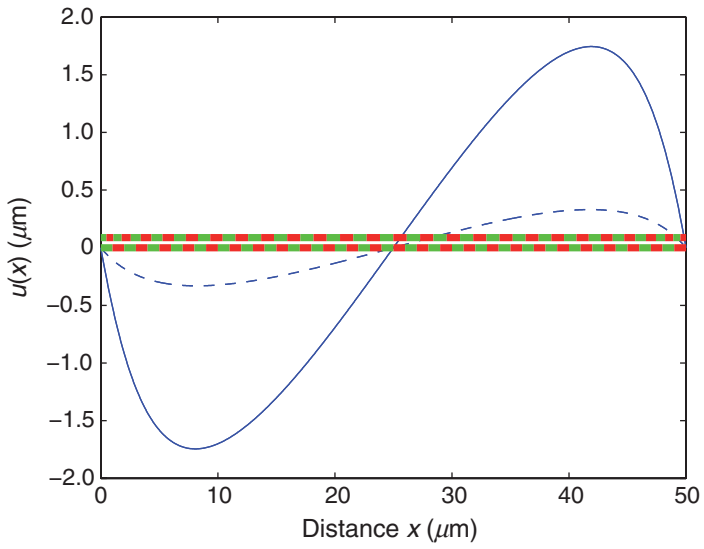

Figure 10. Steady state solution of the displacement $u(x)$ along the fiber before (dashed line) and after (solid line) stimulation with calyculin. The stimulation strongly increases the deformation of the fiber resulting in substantial distortion of the expected striation pattern (upper line) compared to the striation pattern of a completely undistorted fiber (lower line). The upper striation pattern was calculated from the displacement data. The bands close to the boundaries have been contracted (about 55%) whereas the bands around the center have been expanded (about 15%), compare also figure 12.

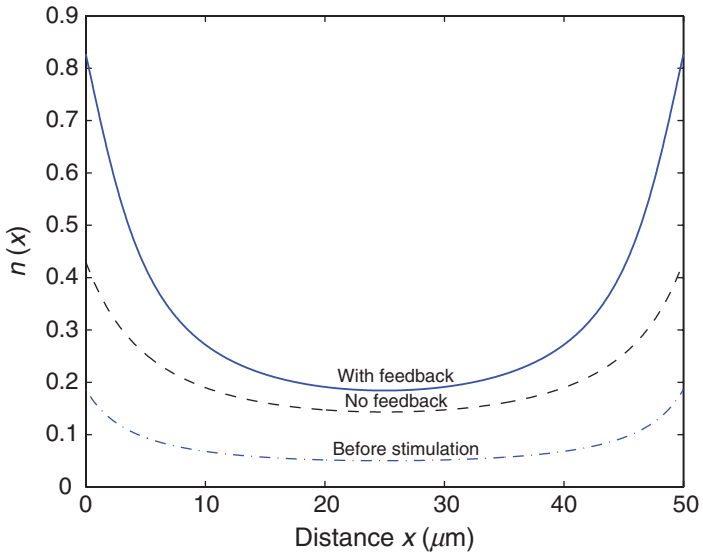

Figure 11. Steady state profile of the active myosin fraction before stimulation with the drug (dash-dotted line), after stimulation including the mechanical feedback (solid line) and after stimulation but neglecting the mechanical feedback (dashed line). For the latter case, homogeneous induction of the drug cause an almost uniform elevation of myosin activity. Slight differences between center and periphery persist but rather marginally extend, whereas the closed feedback system results in an amplification of the spatial differences of myosin activation.

numerical solution for the displacement $u(x, t)$. The steady states of the displacement u before and after stimulation with calyculin are shown in figure 10. The stimulation strongly increases the displacement along the fiber resulting in substantial contraction of the fiber close to the boundaries but in expansion around the cell center. This finding becomes more apparent in the shown striation pattern calculated from the displacement after stimulation (upper string) compared to the striation pattern of a completely undistorted fiber (lower string). The bands close to the boundaries have been contracted whereas the bands around the center have been expanded, compare also figure 13. We have to stress that the presented stress fiber model is continuous, thus the model cannot distinguish between α-actinin bands or MLC bands. The color code in figures 10 and 13 is therefore arbitrary. We also derive the local relative change of density within the fiber which is given in general as the negative trace of the strain tensor $\delta\rho_{\mathrm{rel}} = (\rho - \rho_0)/\rho_0 = -\mathrm{Tr}(u_{i,j})$. Since the model is 1D this simplifies to $\delta\rho_{\mathrm{rel}} = -\partial_x u(x, t)$, plotted in figure 12. The local relative change of band width at a certain position within the fiber, is then simply given by: $(w(x, t) - w_0)/w_0 = -\delta\rho_{\mathrm{rel}}(x, t) = \partial_x u(x, t)$. The figure shows that the inhomogeneous motor activity causes a contraction of the bands up to about 55% close to the fiber ends (the relative change in density is positive), whereas the pattern expands up to 15% at the middle of the fiber (the relative change in density is negative).

The experimental time course data for the sarcomer length shown in figure 2 is intrinsically averaged over a certain area in the peripheral and central regions of the cell. In order to compare the model results with the experimental finding we therefore define central (center $\pm 10\,\mu$m) and peripheral (edges $\pm 10\,\mu$m) regions of the cell, indicated by vertical lines in figure 12.

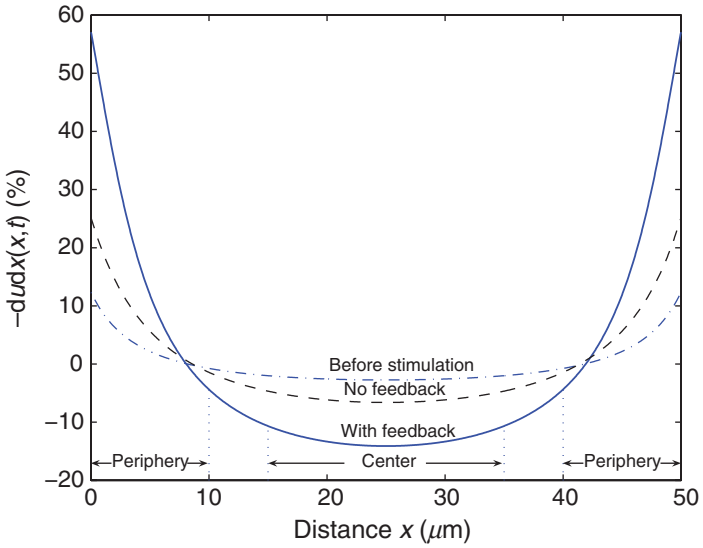

Figure 12. Relative change in density along the fiber in the steady state before stimulation with the drug (dashed-dotted line), after stimulation with the drug including the feedback (solid line) and after stimulation but neglecting the mechanical feedback (dashed line). Positive values correspond to a compression of the fiber, whereas negative values indicate elongation. In case of the closed feedback (solid line) the fiber strongly contracts close to the boundaries up to 55% but elongates at the center to about 15%. In order to compare the model results with the experimental findings, we arbitrarily define central (center $\pm 10\,\mu$m) and peripheral (edges $\pm 10\,\mu$m) regions of the cell, indicated by vertical lines.

The expected sarcomer length at a certain position along the fiber is given by

$$w(x,t) = w_0 + u(x + w_0, t) - u(x,t) \quad \text{or} \quad w(x,t) = w_0\,(1 + \partial_x u(x,t)), \quad \text{for } w_0 \ll L. \quad (22)$$

In the following analysis this measure is averaged over the defined central and peripheral regions, respectively. The deduced time courses for the mean pattern bandwidths in the distinct regions are shown in figure 13. The expected steady state striation patterns are illustrated as insets. Upon stimulation with calyculin, the peripheral mean bandwidth shrinks from its initial value of about $0.97\,\mu$m down to $0.83\,\mu$m, whereas in the central regions, the bands elongate from about $1.03\,\mu$m up to $1.13\,\mu$m. Interestingly, the initial mean bandwidth at the center and periphery yet differ in the initial unperturbed steady state of the cell ($1.03\,\mu$m compared to $0.97\,\mu$m). This results from the fact that the unperturbed fiber already exerts moderate forces on to the focal adhesions which results in slight spatial gradients in myosin activation. These gradients then sharpen upon stimulation with calyculin, see figures 11 and 12. The model results agree qualitatively with the experimental findings by Peterson *et al* [38] and the quantitative measurements are within the same order of magnitude (compare figure 2). It is worth mentioning that the amplitude of contraction or elongation of the fiber scales inversely with the fiber stiffness k: the softer the fiber, the stronger the mechanical deformation will be. Thus, a lower k value would simply explain the reported higher values for sarcomer contraction of about 30–40%.

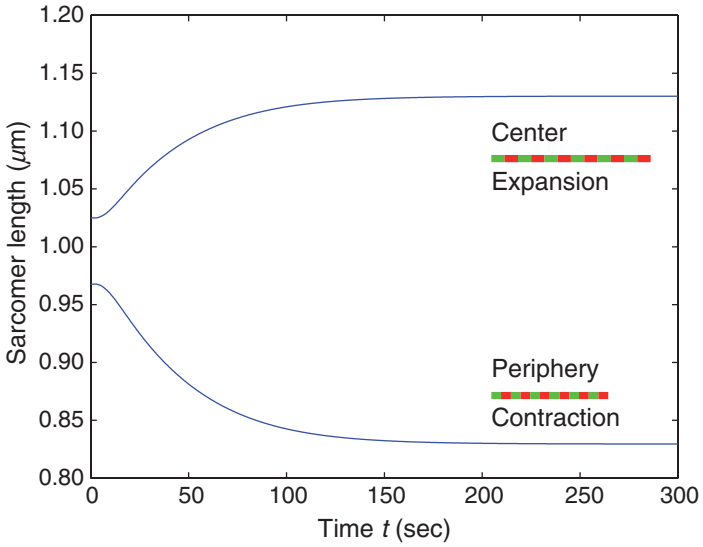

Figure 13. Time courses of the mean bandwidth of the fiber in the center (upper curve) and in the periphery of the cell (lower curve): the shown values are averages of the bandwidths at the center $\pm 10\,\mu$m for the central region and at the edges $\pm 10\,\mu$m for the peripheral region. The defined intervals are also shown in figure 12. The expected steady state striation patterns for the two distinct regions are shown as insets. These results agree qualitatively with the experimental findings by Peterson *et al* shown in figure 2.

In our calculation, we used $k = 45\,\text{nN}\,\mu\text{m}^{-1}$, a value reported by [56]. The experimentally measured equilibration time of the stress fiber upon stimulation is about 20 min (figure 2) which compares to about 3 min for the model results. These quantitative differences originate from two model simplifications. Firstly, we lump the focal adhesion associated processes into one equation thereby we shortcut the activation of ROCK and neglect prior activation steps of e.g. Rho-Gef or Rho-GTPase. Considering these steps would cause an additional time delay. Secondly, the stimulation with calyculin happens instantaneously in the model omitting the time delay caused by the internalization of the drug. Refining the model and eliminating these simplifications will further decrease the differences in equilibration times.

To highlight the importance of the mechanical feedback, we also include the expected results for a system neglecting this feedback shown as dashed lines in figures 11 and 12. Here, the homogeneous induction of the drug causes an almost uniform elevation of myosin activation within the cell. Slight differences between cell center and cell periphery would persist but rather marginally extend (figure 11). In fact stimulation here also leads to amplified distortions of the striation pattern. However, the changes in bandwidths are significantly smaller compared to the system incorporating the feedback (figure 12). Thus the closed biochemical and mechanical feedback loop is an essential feature required to describe the strong distortions of striation patterns upon homogenous drug induction.

6. Conclusion

Here, we have presented for the first time a mathematical model for the closed biochemical–mechanical feedback loop triggering the upregulation of focal adhesions and stress fibers which is typical for cell culture on stiff substrates. In regard to the biochemical part, we present for the first time a reaction–diffusion model for Rho-signaling from focal adhesions towards stress fibers. Our modeling is based on an extensive review of the literature, which provides the list of diffusion and reaction constants summarized in table 3. In regard to the mechanical part, we introduced a new model for stress fibers which takes into account the special viscoelastic and contractile properties of the sarcomeric units. For a linear chain of many such units, we derived a continuum equation which we solved both analytically and numerically. Combining the two model parts resulted in a complete model for the feedback loop of interest. We found that this feedback loop leads to bistability between weak and strong adhesion and to strong spatial gradients in the deformation pattern. In fact, the experimental results can be only explained by incorporating the feedback loop. Our model shows how coupling of mechanics and biochemistry can be modeled in general. In the future, it might be also used to address other issues in the context of cell adhesion, including cell adhesion to soft elastic substrates or to cyclically stretched substrates.

In our model, spatial variations in the deformation pattern result from inhomogeneous reaction–diffusion fields. This prediction should be experimentally tested in the future. Indeed, it has already been reported that MLC-phosphorylation is larger at the periphery than at the center (both before and after stimulation with calyculin) [38], exactly as predicted by our model. Our model does not account for inhomogeneities resulting from spatial variations in mechanical properties (e.g. local accumulation of myosin II, actin or α-actinin), although in principle the model is capable of describing these. A detailed experimental analysis including detailed measurements of local actin and myosin accumulation would be needed to disentangle the relative contributions of biochemical and mechanical factors to the inhomogeneous deformation pattern.

An intriguing aspect of our model is the way different stress fibers might cooperate inside a living cell. Conceptually it is easy to generalize our model to describe a system in which many stress fibers share the signaling input and many focal adhesions share the mechanical output. However, it remains a challenge to model also the dynamics of the actomyosin system if it is not completely condensed into stress fibers.

Acknowledgments

We thank Dominik Meidner for helpful discussions on numerically solving partial differential equations. This work was supported by the Center for Modeling and Simulation in the Biosciences (BIOMS) at Heidelberg.

References

[1] Gumbiner B M 1996 Cell adhesion: the molecular basis of tissue architecture and morphogenesis *Cell* **84** 345–57

[2] Huang S and Ingber D E 1999 The structural and mechanical complexity of cell-growth control *Nat. Cell Biol.* **1** E131–8

[3] Tyson J J, Chen K C and Novak B 2003 Sniffers, buzzers, toggles and blinkers: dynamics of regulatory and signaling pathways in the cell *Curr. Opin. Cell Biol.* **15** 221–31
[4] Kholodenko B N 2006 Cell-signalling dynamics in time and space *Nat. Rev. Mol. Cell Biol.* **7** 165–76
[5] Discher D E, Janmey P and Wang Y-L 2005 Tissue cells feel and respond to the stiffness of their substrate *Science* **310** 1139–43
[6] Vogel V and Sheetz M 2006 Local force and geometry sensing regulate cell functions *Nat. Rev. Mol. Cell Biol.* **7** 265–75
[7] Schwarz U S 2007 Soft matters in cell adhesion: rigidity sensing on soft elastic substrates *Soft Matter* **3** 263–6
[8] Lecuit T and Lenne P-F 2007 Cell surface mechanics and the control of cell shape, tissue patterns and morphogenesis *Nat. Rev. Mol. Cell Biol.* **8** 633–44
[9] Lo C-M, Wang H-B, Dembo M and Wang Y-L 2000 Cell movement is guided by the rigidity of the substrate *Biophys. J.* **79** 144–52
[10] Engler A, Sen S, Sweeney H L and Discher D E 2006 Matrix elasticity directs stem cell lineage specification *Cell* **126** 677–89
[11] Pollard T D and Earnshaw W C 2004 *Cell Biology* 4th edn (Philadelphia, PA: Saunders)
[12] Geiger B, Bershadsky A, Pankov R and Yamada K M 2001 Transmembrane crosstalk between the extracellular matrix and the cytoskeleton *Nat. Rev. Mol. Cell Biol.* **2** 793–805
[13] Bershadsky A, Balaban N Q and Geiger B 2003 Adhesion-dependent cell mechanosensitivity *Annu. Rev. Cell Dev. Biol.* **19** 677–95
[14] Zaidel-Bar R, Itzkovitz S, Ma'ayan A, Iyengar R and Geiger B 2007 Functional atlas of the integrin adhesome *Nat. Cell Biol.* **9** 858–67
[15] Ridley A J and Hall A 1992 The small GTP-binding protein Rho regulates the assembly of focal adhesions and actin stress fibers in response to growth factors *Cell* **70** 389–99
[16] Ridley A J, Paterson H F, Johnston C L, Diekmann D and Hall A 1992 The small GTP-binding protein Rac regulates growth factor-induced membrane ruffling *Cell* **70** 401–10
[17] Sander E E, ten Klooster J P, van Delft S, van der Kammen R A and Collard J G 1999 Rac downregulates Rho activity: reciprocal balance between both GTPases determines cellular morphology and migratory behavior *J. Cell Biol.* **147** 1009–22
[18] Burridge K and Wennerberg K 2004 Rho and Rac take center stage *Cell* **116** 167–79
[19] Hall A 1998 Rho GTPases and the actin cytoskeleton *Science* **279** 509–14
[20] Etienne-Manneville S and Hall A 2002 Rho GTPases in cell biology *Nature* **420** 629–35
[21] Riveline D, Zamir E, Balaban N Q, Schwarz U S, Geiger B, Kam Z and Bershadsky A D 2001 Focal contact as a mechanosensor: externally applied local mechanical force induces growth of focal contacts by a mDia1-dependent and ROCK-independent mechanism *J. Cell Biol.* **153** 1175–85
[22] Nicolas A, Geiger B and Safran S A 2004 Cell mechanosensitivity controls the anisotropy of focal adhesions *Proc. Natl. Acad. Sci. USA* **101** 12520–25
[23] Nicolas A and Safran S A 2004 Elastic deformations of grafted layers with surface stress *Phys. Rev.* E **69** 051902
[24] Shemesh T, Geiger B, Bershadsky A D and Kozlov M M 2005 Focal adhesions as mechanosensors: a physical mechanism *Proc. Natl. Acad. Sci. USA* **102** 12383–88
[25] Besser A and Safran S A 2006 Force-induced adsorption and anisotropic growth of focal adhesions *Biophys. J.* **90** 3469–84
[26] Raz-Ben Aroush D and Wagner H D 2006 Shear-stress profile along a cell focal adhesion *Adv. Mater.* **18** 1537–40
[27] Nicolas A and Safran S A 2006 Limitation of cell adhesion by the elasticity of the extracellular matrix *Biophys. J.* **91** 61–73
[28] Bershadsky A, Kozlov M and Geiger B 2006 Adhesion-mediated mechanosensitivity: a time to experiment, and a time to theorize *Curr. Opin. Cell Biol.* **18** 472–81

[29] Novak I L, Slepchenko B M, Mogilner Al and Loew L M 2004 Cooperativity between cell contractility and adhesion *Phys. Rev. Lett.* **93** 268109
[30] Civelekoglu-Scholey G, Wayne Orr A, Novak I, Meister J-J, Schwartz M A and Mogilner A 2005 Model of coupled transient changes of Rac, Rho, adhesions and stress fibers alignment in endothelial cells responding to shear stress *J. Theor. Biol.* **232** 569–85
[31] Deshpande V S, McMeeking R M and Evans A G 2006 A bio-chemo-mechanical model for cell contractility *Proc. Natl Acad. Sci. USA* **103** 14015–20
[32] McMeeking R M, Deshpande V S and Evans A G 2007 A model for the contractility of the cytoskeleton including the effects of stress-fibre formation and dissociation *Proc. R Soc.* A **463** 787–815
[33] Huxley A F 1957 Muscle structure and theories of contraction *Prog. Biophys. Chem.* **7** 255–318
[34] Mijailovich S M, Fredberg J J and Butler J P 1996 On the theory of muscle contraction: filament extensibility and the development of isometric force and stiffness *Biophys. J.* **71** 1475–84
[35] Duke T A J 1999 Molecular model of muscle contraction *Proc. Natl Acad. Sci. USA* **96** 2770–5
[36] Kruse K and Jülicher F 2000 Actively contracting bundles of polar filaments *Phys. Rev. Lett.* **85** 1778–81
[37] Kruse K and Jülicher F 2003 Self-organization and mechanical properties of active filament bundles *Phys. Rev.* E **67** 051913
[38] Peterson L J, Rajfur Z, Maddox A S, Freel C D, Chen Y, Edlund M, Otey C and Burridge K 2004 Simultaneous stretching and contraction of stress fibers *in vivo Mol. Biol. Cell* **15** 3497–508
[39] Seabra M C 1998 Membrane association and targeting of prenylated Ras-like GTPases *Cell. Signal.* **10** 167–72
[40] Somlyo A P and Somlyo A V 2000 Signal transduction by G-proteins, Rho-kinase and protein phosphatase to smooth muscle and non-muscle myosin II *J. Physiol.* **522** 177–85
[41] Feng J *et al* 1999 Rho-associated kinase of chicken gizzard smooth muscle *J. Biol. Chem.* **274** 3744–52
[42] Kamm K E and Stull J T 1985 The function of myosin and myosin light chain kinase phosphorylation in smooth muscle *Annu. Rev. Pharmacol.* **25** 593–620
[43] Murray J D 2002 *Mathematical Biology* (New York: Springer)
[44] Klipp E, Herwig R, Kowald A, Wierling C and Lehrach H 2005 *Systems Biology in Practice. Concepts, Implementation and Application* (Weinheim: Wiley-VCH)
[45] Kumar S, Maxwell Iva Z, Heisterkamp A, Polte T R, Lele T P, Salanga M, Mazur E and Ingber D E 2006 Viscoelastic retraction of single living stress fibers and its impact on cell shape, cytoskeletal organization, and extracellular matrix mechanics *Biophys. J.* **90** 3762–73
[46] Hartshorne D J, Ito M and Erdoedi F 1998 Myosin light chain phosphatase: subunit composition, interactions and regulation *J. Muscle Res. Cell Motil.* **19** 325–41
[47] Nagamoto H and Yagi K 1984 Properties of myosin light chain kinase prepared from rabbit skeletal muscle by an improved method *J. Biochem.* **95** 1119–30
[48] Butler T M, Narayan S R, Mooers S U and Siegman M J 1994 Rapid turnover of myosin light chain phosphate during cross-bridge cycling in smooth muscle *Am. J. Physiol.—Cell Physiol.* **267** C1160–66
[49] Amano M, Ito M, Kimura K, Fukata Y, Chihara K, Nakano T, Matsuura Y and Kaibuchi K 1996 Phosphorylation and activation of myosin by Rho-associated kinase (Rho-kinase) *J. Biol. Chem.* **271** 20246–9
[50] Hathaway D R and Adelstein R S 1979 Human platelet myosin light chain kinase requires the calcium-binding protein calmodulin for activity *Proc. Natl Acad. Sci. USA* **76** 1653–7
[51] Nunnally M H, Rybicki S B and Stull J T 1985 Characterization of chicken skeletal muscle myosin light chain kinase. Evidence for muscle-specific isozymes *J. Biol. Chem.* **260** 1020–6
[52] Bartelt D C, Moroney D J and Wolff S 1987 Purification, characterization and substrate specificity of calmodulin-dependent myosin light-chain kinase from bovine brain *Biochem. J.* **247** 747–56
[53] Pato M D and Adelstein R S 1983 Purification and characterization of a multisubunit phosphatase from turkey gizzard smooth muscle. The effect of calmodulin binding to myosin light chain kinase on dephosphorylation *J. Biol. Chem.* **258** 7047–54

[54] Lippincott-Schwartz J, Snapp E and Kenworthy A 2001 Studying protein dynamics in living cells *Nat. Rev. Mol. Cell Biol.* **2** 444–56
[55] Umemoto S and Sellers JR 1990 Characterization of in vitro motility assays using smooth muscle and cytoplasmic myosins *J. Biol. Chem.* **265** 14864–9
[56] Deguchi S, Ohashi T and Sato M 2006 Tensile properties of single stress fibers isolated from cultured vascular smooth muscle cells *J. Biomech.* **39** 2603–10
[57] Balaban N Q *et al* 2001 Force and focal adhesion assembly: a close relationship studied using elastic micropatterned substrates *Nat. Cell Biol.* **3** 466–72
[58] Fung Y C 1993 *Biomechanics: Mechanical Properties of Living Tissues* (New York: Springer)
[59] Schwarz U S, Erdmann T and Bischofs I B 2006 Focal adhesions as mechanosensors: the two-spring model *BioSystems* **83** 225–32